

Poly(caprolactone)/clay masterbatches prepared in supercritical CO₂ as efficient clay delamination promoters in poly(styrene-*co*-acrylonitrile)

Laetitia Urbanczyk,^a Cédric Calberg,^b Samira Benali,^c Serge Bourbigot,^d Eliane Espuche,^e Fabrice Gouanvé,^e Philippe Dubois,^{ef} Albert Germain,^b Christine Jérôme,^a Christophe Detrembleur^{*a} and Michael Alexandre^a

Received 30th April 2008, Accepted 16th July 2008

First published as an Advance Article on the web 21st August 2008

DOI: 10.1039/b807357k

Poly(styrene-*co*-acrylonitrile) (SAN)/clay nanocomposites with a high degree of clay exfoliation were prepared upon melt blending of pre-exfoliated poly(ϵ -caprolactone) (PCL)/organoclay masterbatches in a Brabender-type internal mixer. These highly filled masterbatches were synthesized by a one-pot process using supercritical carbon dioxide as a polymerization medium. During their dispersion into SAN, PCL is expected to act as a compatibilizer at the polymer–clay interface as it is miscible with the host matrix under these conditions. Reference nanocomposites based on direct melt mixing of the commercial organoclay were also prepared for the sake of comparison. The superiority of the masterbatch route in term of clay delamination efficiency has been evidenced by XRD analysis, visual and TEM observations. The effect of the nanocomposite morphology on the polymer properties was then investigated. A substantial improvement of the fire behaviour and a decrease in gas permeability have been observed for the nanocomposite containing the highest level of clay exfoliation, accompanied with a higher brittleness as evidenced by traction and impact tests.

Introduction

Polymer/lamellar clay nanocomposites have received significant attention, both in industry and in academia during the last two decades. Indeed, the introduction of a small amount of well-dispersed nanoclay (~3–5 wt%) into a polymer matrix increases considerably several matrix properties such as mechanical and thermal properties, gas permeability, flame retardancy *etc.*¹ The challenge remains to efficiently delaminate the clay sheets in order to obtain the best property enhancement. Several strategies have been envisioned to incorporate nanoclays into polymers, such as solvent intercalation, *in situ* intercalative polymerization or melt blending. The latter is the preferred method from an industrial point of view, because it is rather simple and uses existing equipment and technologies. However, the complete exfoliation and homogeneous dispersion of silicate layers have been achieved only in a small number of cases by this way, such as adequately organomodified montmorillonite into polyamide-6.² *In situ*

intercalative polymerization has proven to be more effective in delaminating the clay sheets into many polymers such as in poly(ϵ -caprolactone) (PCL),³ poly(lactide) (PLA),⁴ and poly(propylene) (PP),⁵ but the presence of nanoclay often interferes with the polymerization course, influencing to a large extent the molecular parameter of the resulting matrix.

In this article, our interest will be devoted to poly(styrene-*co*-acrylonitrile) (SAN) as the host polymer. This matrix has been chosen because of several interesting properties such as good mechanical and chemical resistance, optical transparency, and ease of processing.

Several papers have dealt with the preparation of SAN/clay nanocomposites. A few of them reported the synthesis of the polymer *in situ* in the presence of an organomodified clay in organic solvents (*e.g.* THF)⁶ or natural Na⁺–MMT in emulsion in water.^{7,8} The polymer is mostly intercalated into the clay layers in the first case whereas a good clay exfoliation degree was obtained in the second case. However, the preparation of these nanocomposites by the melt-blending technique is the most important of those reported in the literature, because it is a more straightforward process allowing one to work with commercial matrices. Stretz *et al.*,⁹ Chu *et al.*¹⁰ and Jang *et al.*¹¹ have melt-mixed SAN with different organoclays to evaluate the effect of the clay organomodifier (onium surfactants) on the final morphology. Intercalated to nearly exfoliated morphologies were obtained depending on the surfactant, with a minimum of three clay layers per stack in the best case. Some authors^{10,12,13} have studied the effect of the acrylonitrile (AN) content on the clay dispersion. Stretz and Paul¹² have observed a better organoclay delamination with a higher AN content. However, it appeared that too high a AN content (>40 wt%) is detrimental to exfoliation. An increase in AN content leads to an increase in polarity and also in viscosity. Both factors are believed to have some impact on the degree of particle dispersion.

^aCenter for Education and Research on Macromolecules (CERM), University of Liège, Sart-Tilman B6a, 4000 Liège, Belgium. E-mail: Christophe.Detrembleur@ulg.ac.be; Fax: +32 4366 3496; Tel: +32 4366 3465

^bDepartment of Applied Chemistry, University of Liège, Sart-Tilman B6a, 4000 Liège, Belgium

^cCenter of Innovation and Research in Material & Polymers CIRMAP, Laboratory of Polymeric and Composite Materials, University of Mons-Hainaut, Académie Universitaire Wallonie-Bruxelles, Place du Parc 20, B-7000 Mons, Belgium

^dEquipe Procédés d'Elaboration de Revêtements Fonctionnels, LSPES UMR-CNRS 8008, ENSCL, BP 90108, 59652 Villeeneuve d'Ascq Cedex, France

^eLaboratoire des Matériaux Polymères et des Biomatériaux, UMR 5223, Université Claude Bernard Lyon 1, Bât ISTIL, 15 Bd A. Latarjet, 69622 Villeurbanne Cedex, France

^fMateria Nova asbl, Parc Initialis, Av. Nicolas Copernic n°1, 7000 Mons, Belgium

Another strategy to enhance the clay dispersion is the partial methylsilylation of the OH groups on the clay surface.¹⁴ Indeed, the authors believe that when the polymer has been inserted between the clay sheets, it is “glued” in an intercalated state because of strong interactions between the polymer and the clay surface. The methylsilylation decreases the number of clay surface OH groups, and so reduces the strong interactions responsible for the glue effect. When a shear force is applied, the silicate layers slide more easily on each other and give a higher degree of clay dissociation.

Kim *et al.*¹⁵ and Kiersnowski and Piglowski¹⁶ have used poly(ϵ -caprolactone) (PCL) as a compatibilizing agent, as this polymer is known to be completely miscible with SAN, when the AN content in the SAN copolymer lies between 8 and 28 wt%.¹⁷ They prepared PCL/clay masterbatches either by melt blending¹⁵ or *in situ* polymerization in bulk.¹⁶ This binary mixture was then dispersed into SAN. The clay delamination into SAN has shown to be enhanced by these techniques even though conditions have not been optimized yet.

A masterbatch route where polymer or oligomer chains, identical or miscible with the polymer matrix, and anchored onto the clay surface through ionic bonds has already proven to be an efficient technique for clay dispersion into poly(vinyl chloride) (PVC),¹⁸ PLA,⁴ and chlorinated polyethylene.^{19,20}

The goal of this work is to study PCL/clay masterbatches prepared by *in situ* intercalative polymerization in supercritical carbon dioxide²¹ as efficient systems for the preparation of exfoliated nanocomposite in a SAN matrix, chosen as an amorphous glassy matrix. Such masterbatches have already shown their efficiency upon dispersion into chlorinated polyethylene,^{19,20} a rubber-like slightly crystalline matrix.

Supercritical carbon dioxide (scCO₂), used as solvent, is a unique medium because of several interesting properties, such as low viscosity combined with high diffusivity. This allows the production of masterbatches with high inorganic content (up to 50 wt% in inorganics) without viscosity problems, such as those encountered when the synthesis of such masterbatches is conducted in bulk, which limits the inorganic clay loading to a maximum value of ~25 wt%. Furthermore, an easily recoverable fine powder can be obtained after depressurization, which is a huge advantage compared to the classical bulk synthesis where the masterbatches are recovered as solid blocks that need to be re-processed (grinding followed by vacuum drying or solubilisation/precipitation to eliminate residual monomer) before use. The dispersion efficiency into SAN will be characterized by visual appearance, TEM and XRD and related to the resulting mechanical, fire retardant and gas barrier properties.

Experimental

Materials

ϵ -Caprolactone (ϵ -CL) and bis(2-ethylhexanoate) tin(II) (Sn(oct)₂), from Sigma-Aldrich (95%), were dried over molecular sieves for 48 h prior to use. The CO₂ used came from Air Liquide Belgium and was pure at 99.995%. Two different clays were selected from Southern Clay Products (Texas, USA). These montmorillonite clays were organomodified either with dimethyl(dihydrogenated tallowalkyl) ammonium cation (Cloisite®

Table 1 Characteristics of the commercial clays and the PCL/clay masterbatches synthesized in scCO₂

Filler	Cation	PCL fraction /wt% ^a	PCL molecular weight ^b /g mol ⁻¹	Inorganic fraction/wt % ^a	Interlayer spacing/nm ^c
Cloisite® 20A	(CH ₃) ₂ N ⁺ (HT) ^d	—	—	71	1.9
Cloisite® 30B	(C ₂ H ₄ OH) ₂ N ⁺ (T) ^e CH ₃	—	—	80	1.7
MB-20A	(CH ₃) ₂ N ⁺ (HT)	50	3900	32.5	3.5
MB-30B	(C ₂ H ₄ OH) ₂ N ⁺ (T)CH ₃	34	1500	53	3.2

^a Determined by thermogravimetric analysis under air at 20 K min⁻¹, residue at 800 °C. ^b Determined by size exclusion chromatography using polystyrene standards and using the formula $M_{n,PCL} = 0.259 \times M_{n,PS}^{1.073}$. ^c Determined by X-ray diffraction. ^d HT= hydrogenated tallow with ~65% C₁₈, ~30% C₁₆, ~5% C₁₄. ^e T= tallow with ~65% C₁₈, ~30% C₁₆, ~5% C₁₄.

20A) or with bis-(2-(hydroxyethyl)methyl)(tallowalkyl) ammonium cation (Cloisite® 30B). The poly(styrene-*co*-acrylonitrile) (SAN) matrix, Luran®358N, was provided by BASF. The AN content was 25 wt%. Low molecular weight PCL ($M_n = 4000$ g mol⁻¹), CAPA®2402, was kindly offered by Solvay.

The synthesis of PCL/clay masterbatches in scCO₂ has been fully described in a previous paper.¹⁹ Typically, polymerization was conducted in a 100 mL stainless-steel high pressure reactor. The clay was dried in the reactor under vacuum at 85 °C for 1 night and then dry ϵ -CL was introduced under nitrogen flow, followed by Sn(oct)₂. Polymerization was then carried out for 7 days in CO₂ under supercritical conditions (85 °C, 280 bar in CO₂). The reactor was then cooled down to room temperature and depressurized to collect the masterbatch as a fine beige powder. The composition of the clays and masterbatches used in this study are detailed in Table 1.

Melt-blending process

The clays, the masterbatches or the PCL are melt-blended with the molten SAN matrix in a counter-rotating twin-screw internal mixer (Brabender®). The melt mixing is performed at 175 °C for 5 minutes with a roller blade screw rotation speed of 75 rpm. The samples are then molded into a 3 mm-thick sample in a hot press (175 °C) for 5 minutes for characterization.

Characterization

Thermogravimetric analysis (TGA) of the samples has been carried out on a TA Instrument Q500 model, under air or He flow, with a heating rate of 20 K min⁻¹, in an open platinum pan. Measurements have been performed in triplicate, and precision on temperature lies around 0.5%.

X-Ray diffraction analysis (XRD) was carried out with a powder diffractometer Siemens D5000 (Cu K α radiation with $\lambda = 0.15406$ nm, 50 kV, 40 mA, Ni filter, $\theta/2\theta$ geometry) at room temperature for 2θ varying from 1.65° to 30° by 0.04° steps, in order to characterize the final nanocomposites morphology.

Organic fractions (poly(ϵ -caprolactone) and ammonium salts) have been extracted from masterbatches by an ion-exchange reaction between the ammonium functions and lithium cations, by mixing a few grams of the nanocomposite in a THF solution saturated with LiCl. After 48 h, the clay was separated from the solution by filtration and the liquid fraction was concentrated and then precipitated in a ten-fold quantity of *n*-heptane. The polymer was recovered and the average molar mass of PCL was determined by size exclusion chromatography (SEC) in THF at 45 °C at a flow rate of 1 mL min⁻¹ with a SFD S5200 autosampler liquid chromatograph equipped with a SFD refractometer index detector 2000. PL gel 5 μ m (10⁵, 10⁴, 10³ and 100 Å) columns were calibrated with polystyrene standards. The universal calibration curve was set up on the basis of the viscosimetric relationships for PS and PCL ($[\eta]_{\text{PS}} = 1.25 \times 10^{-4} M^{0.717}$, $[\eta]_{\text{PCL}} = 1.09 \times 10^{-3} M^{0.6}$). The extraction of organics (PCL + ammonium salts) from the masterbatch was quantitative within ~10% according to TGA analysis made on the clays recovered after ion exchange.

Clay delamination efficiency was directly observed by transmission electron microscopy (TEM, Philips CM100). Ultrathin sections (50–80 nm) were prepared with an Ultramicrotome Ultracut FC4e, Reichert-Jung. No staining was used since the aluminosilicate sheets are contrasting enough in the polymer matrix.

The glass transition temperature (T_g) of each sample was determined with a TA 2010 DSC thermal analyzer calibrated with indium. Samples were encapsulated in aluminium pans and the following cycle was used: heating from room temperature to 120 °C, at 10 K min⁻¹ and then cooling to 0 °C, and then this cycle was repeated. The measurements were performed in triplicate and the average T_g value is reported.

Tensile tests were performed with a Lloyd LR 10 K tensile testing apparatus. Tensile properties were measured at 20 °C with a constant deformation rate of 10 mm min⁻¹ on dumbbell-shaped specimens prepared from compression-molded samples according to the 638 type V ASTM norm. Tensile data were evaluated on the average of five independent measurements.

Charpy impact strength was measured with a Zwick pendulum impact tester at 20 °C according to the norm ISO 179–1. The size of the specimens was 63 × 12 × 3 mm, with a rectangular notch size of 2 mm deep and 1 mm large. The impact energy promoted by the hammer was 0.5 J. The impact strength values were evaluated on the average of five independent measurements.

Combustion behaviour was assessed according to the ASTM E 906 procedure in a Fire Testing Technology Limited Instruments mass loss cone calorimeter. The equipment is identical to that used in oxygen-consumption cone calorimetry (ASTM E-1354-90), except that a thermopile in a chimney is used to obtain heat release rate (HRR) rather than employing the oxygen-consumption principle. Mass loss readings are performed simultaneously by ASTM E-1354, and serve as a benchmark of the heat release rate values obtained in this manner. The measurements have been performed at a heat flux of 35 kW m⁻², using a cone-shaped heater. The samples (100 × 100 × 3 mm) in horizontal orientation were subjected to a spark until the sample was ignited. The aim was to simulate the conditions likely to occur in a real fire (small fire scenario). When measured at 35 kW m⁻², HRR is reproducible to within <10%. The cone data reported in this paper are the average of three replicated experiments.

Gas permeation experiments were carried out for He, O₂ and CO₂ at 20 °C under an upstream pressure equal to 3 bar. The polymer and nanocomposites samples were pressed at 175 °C to produce 20 μ m thick membranes. The permeation cell consisted of two compartments separated by the studied membrane. The pressure variations in the downstream compartment were measured as a function of time. The permeability coefficient P expressed in Barrer units was calculated from the slope of the straight line in the steady state. The precision on P values was better than 5%.

Results and discussion

Clay dispersion into SAN: morphology characterization

The commercial clays Cloisite® 20A (Cl20A) and Cloisite® 30B (Cl30B), as well as the home-made masterbatches resulting from ϵ -caprolactone polymerization in scCO₂ in the presence of the same clays have been melt-mixed into SAN in an internal mixer. The compositions are summarized in Table 2. As the SAN matrix is translucent, the quality of clay dispersion can be visualised directly (Fig. 1) on the 3 mm-thick compression-molded samples.

A lot of small clay stacks appear in the direct-mixed nanocomposites, which are cloudy, whereas the masterbatch-mixed nanocomposites are translucent and completely devoid of visible clay stacks. So the difference in terms of clay dispersion between the two kinds of samples is huge. It is worth noting that discoloration of the samples is strongly related to the nature of the clay organomodifier, where more brown samples are observed for Cloisite® 30B.

Table 2 Composition and characteristics of SAN and SAN/clay nanocomposites. DM stands for direct-mixed and MB for masterbatch-mixed

Code	Type of clay	wt% clay (inorganic fraction)	Aspect	Interlayer spacing/nm
Ref-SAN	—	0	Translucent	No XRD signal
SAN-DM20A	20A	3	Opaque	3.4
SAN-MB20A	20A	3	Translucent	3.4
SAN-DM30B	30B	3	Opaque	3.5
SAN-MB30B	30B	3	Translucent	Very weak XRD signal



Fig. 1 Optical transparency of SAN and SAN/clay nanocomposites on 3 mm-thick compression-molded samples. DM stands for direct-mixed and MB for masterbatch-mixed.

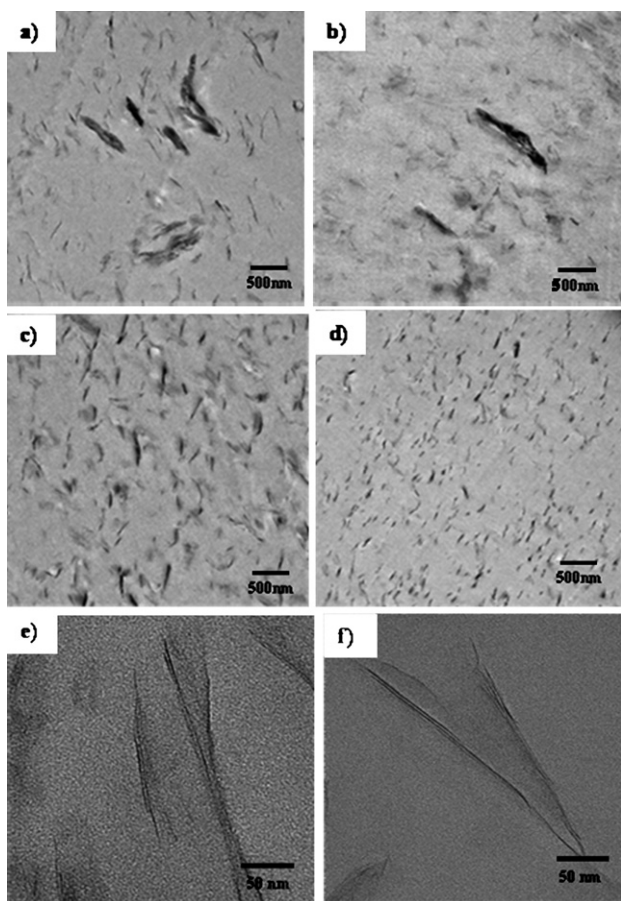


Fig. 2 TEM images of SAN/clay nanocomposites containing 3 wt% of clay (inorganic fraction): a) SAN-DM20A, b) SAN-DM30B, c) SAN-MB20A, d) SAN-MB30B, e) SAN-MB20A (higher magnification), and f) SAN-MB30B (higher magnification).

The extent of clay delamination of the pressed samples has been microscopically assessed using TEM analysis (Fig. 2). Some intercalated stacks are clearly observed in direct-mixed (DM) composites (Fig. 2a,b), surrounded by delaminated sheets. These nanocomposites can then be qualified as semi-intercalated/semi-exfoliated nanocomposites. The masterbatch-mixed (MB) nanocomposites show a very efficient clay delamination without remaining stacks (Fig. 2c,d). The sheets are homogeneously dispersed throughout the matrix and the clay sheets are well separated from each other, however not totally exfoliated, since besides individual clay sheets, very small stacks of 2 to 6 clay sheets can still be observed (Fig. 2e,f).

Fig. 3 shows the XRD patterns for SAN, Cloisite® 20A, Cloisite® 30B, and the different SAN/clay nanocomposites. The diffraction peaks at low 2θ angle, typical of intercalated clay structures, appear with a high intensity for the direct-mixed nanocomposites.

The clay interlayer distance of SAN-DM20A and SAN-DM30B, calculated according to Bragg's law, is increased (3.4–3.5 nm) compared to the neat organoclays (1.9–1.7 nm), proving the SAN intercalation between the clay sheets, but the overall structure is still regular. Unlike the direct-mixed nanocomposites, the masterbatch-mixed ones are characterized by

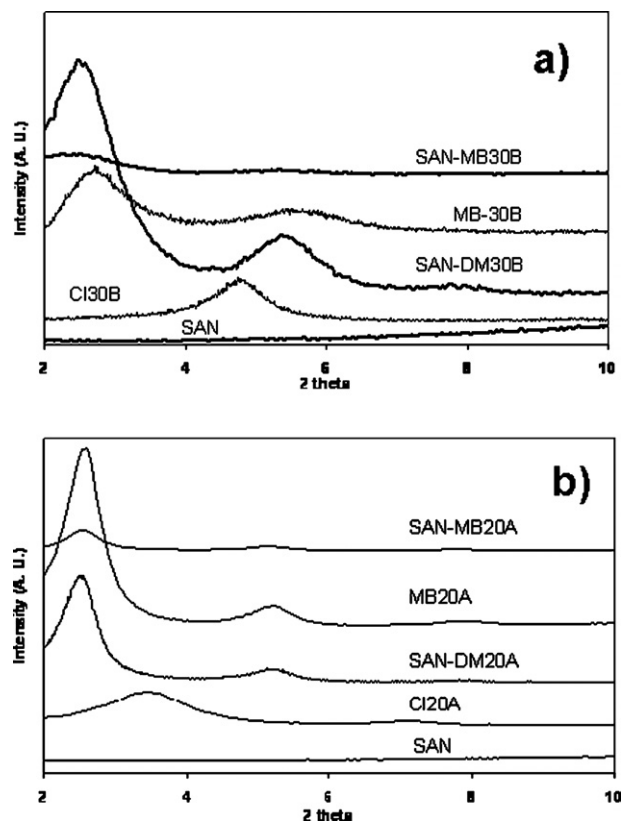


Fig. 3 XRD patterns of SAN, Cloisite® 20A, Cloisite® 30B, and SAN/clay nanocomposites containing 3 wt% of clay (inorganic fraction).

a broad signal in the low 2θ angle with a very low intensity. This is typical of a disordered system with a high level of clay exfoliation, however not totally exfoliated.

Mechanical properties

The tensile properties of the samples have been tested with a Lloyd LR 10 K tensile testing apparatus under traction. Fig. 4 shows the Young's modulus and elongation at break for each sample. The Young's modulus remains constant in SAN-DM30B and SAN-MB20A nanocomposites compared to the pure polymer, whereas it increases slightly for SAN-MB30B

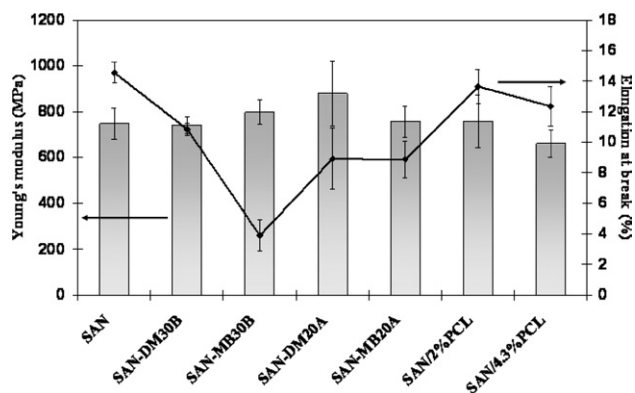


Fig. 4 Tensile properties of SAN, SAN/clay nanocomposites (3 wt% clay) and SAN/PCL binary mixtures.

(+6%) and SAN-DM20A (+18%) nanocomposites. However, the elongation at break of the nanocomposites decreases sharply compared to SAN, down to 27% from the initial value for the SAN-MB30B sample. This decreased ductility is common especially for brittle polymers after incorporating a rigid filler.²¹ It might arise, particularly for SAN-MB30B, from a lack of interfacial reinforcement between SAN and grafted PCL due to the absence of entanglements between the polymer chains coming from the low molecular weight of the grafted PCL. We have also tested binary mixtures of SAN/PCL ($M_{n,PCL} = 4000 \text{ g mol}^{-1}$) to see the influence of the polyester on material mechanical properties. 2 wt% and 4.3 wt% of the polyester have been introduced into SAN, to match the PCL content contained in SAN-MB30B and SAN-MB20A nanocomposites, respectively. The mechanical properties do not seem to be influenced with the introduction of 2 wt% of PCL, whereas a slight decrease in both Young's modulus (−12%) and elongation at break (−15%) are observed with 4.3 wt% of PCL.

In conclusion, the addition of a few percent of nanoclay and/or low molecular weight PCL into SAN has no significant influence on the material stiffness under traction but makes the material more brittle.

Charpy impact testing has been performed on the same samples to quantify more adequately the effect of clay and/or PCL addition on material brittleness (Fig. 5). We observe a decrease of the impact strength for all the nanocomposites, with a drop from 7 to 48% compared to SAN impact strength value. A similar behaviour had already been reported for other matrix/clay nanocomposites such as ABS,²¹ PCL²² or HDPE²³ and may be related to the interfacial effects at the filler–polymer matrix interface.

The difference between SAN-DM30B and SAN-DM20A impact strength values is certainly related to a lower affinity between the non-functional organomodifier contained in Cloisite® 20A and the matrix compared to the functional one (two hydroxyl groups) in Cloisite® 30B, more compatible with SAN (possibility of H-bonding between the nitrile group of SAN and the hydroxyl groups of the organomodifier). The increased brittleness of the masterbatch-redispersed nanocomposites compared to the direct-mixed ones are mainly due to the higher interfacial surface between the clay and the matrix as a result of

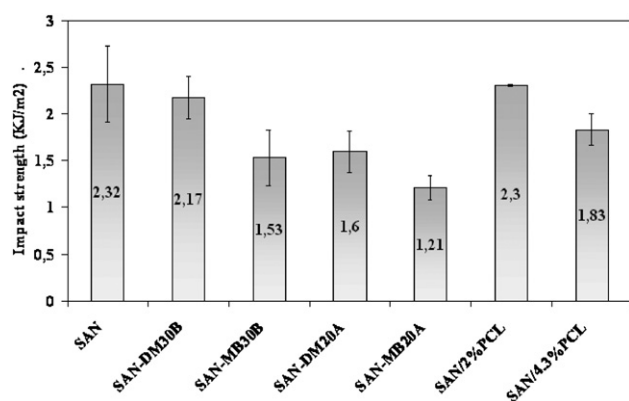


Fig. 5 Impact properties (Charpy) of SAN, SAN/clay nanocomposites (3 wt% clay) and SAN/PCL binary mixtures.

the high degree of sheets delamination. The well-dispersed nanoclays are thus more prone to induce such brittleness.

As previously observed by traction test, SAN ultimate properties remain unchanged with the addition of 2 wt% of PCL whereas it decreases (−20%) with 4.3 wt% of PCL upon impact testing. PCL seems thus to act as an antiplasticizer.²⁴ This phenomenon has already been described in the literature with different systems such as polycarbonate-PCL²⁵ or PS-mineral oil.²⁶ In these papers, they explain the material ultimate properties drop by a reduction of free volume and restriction of polymer molecular mobility due to the low molecular weight additive incorporated, the effect being more pronounced with a higher amount of additive.

We should mention that in this study, the filler addition into SAN was attempted not to increase the material mechanical properties, as SAN is already stiff, but to enhance other properties like thermal properties, fire resistance and to decrease gas permeability.

Thermal properties

The prepared nanocomposites have been analysed by differential scanning calorimetry (DSC). It is worth noting that no melting endotherm arising from the presence of PCL in the SAN nanocomposite samples based on masterbatches is observed in the DSC traces, indicating the absence of PCL demixing. The SAN glass transition temperature (T_g) obtained for the different nanocomposites are gathered in Table 3, as well as the PCL content introduced in each sample. The SAN T_g (105 °C) is almost unchanged in the SAN/clay direct-mixed nanocomposites, whereas it decreases in the masterbatch-blended ones, due to the presence of the PCL. The drop is more pronounced for the SAN-MB20A sample, because of the higher PCL content incorporated in this nanocomposite. The theoretical T_g values can be calculated with the Fox equation for a binary polymer blend: $1/T_g = w_1/T_{g1} + w_2/T_{g2}$, with w_x being the weight fraction of the component x, and $T_{g1} = 378 \text{ K}$ (SAN) and $T_{g2} = 213 \text{ K}$ (PCL). The experimental T_g value for SAN-MB20A fits the theory whereas SAN-MB30B measured T_g is higher than the calculated one. This may be explained by a smaller effect of PCL chains on T_g arising from their partial grafting onto the clay surface.

The thermal stability of SAN and the nanocomposites based on Cloisite® 30B were studied by thermogravimetric analysis. The measurements have been performed under air and under helium. The data for the polymer and its nanocomposites under air and helium are shown in Fig. 6 and 7, respectively, and

Table 3 Glass transition temperature of SAN/clay nanocomposites measured by differential scanning calorimetry

Sample	$T_g/^\circ\text{C}$	PCL content/wt %	Theoretical $T_g/^\circ\text{C}^a$
SAN	105	—	—
SAN-DM20A	106	—	—
SAN-MB20A	94	4.3	93
SAN-DM30B	105	—	—
SAN-MB30B	102	2	99

^a Glass transition temperature expected from the Fox equation.

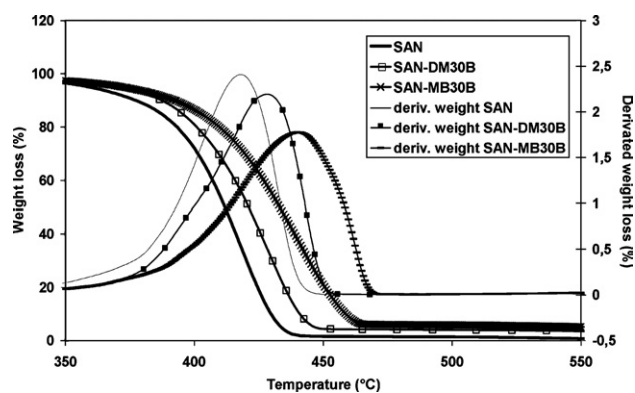


Fig. 6 Thermogravimetric analysis curves of SAN and SAN/clay nanocomposites (3 wt% clay) under air, at 20 °C min⁻¹.

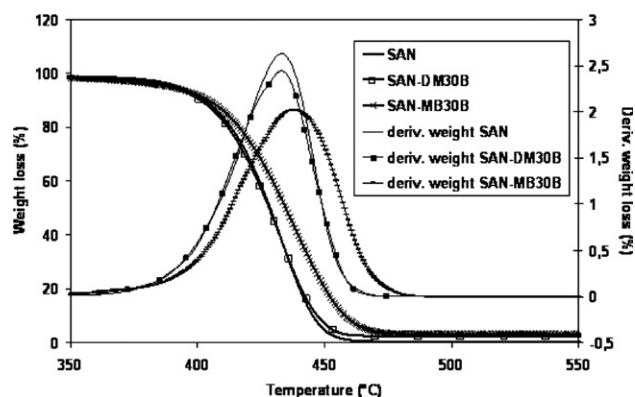


Fig. 7 Thermogravimetric analysis curves of SAN and SAN/clay nanocomposites (3 wt% clay) under helium, at 20 °C min⁻¹.

Table 4 summarizes the position of the maximum derivated weight loss peaks. Under air, a shift of the decomposition temperature towards higher values for the nanocomposites can be observed, compared to SAN. The highest shift corresponds to the well dispersed nanocomposite, with a delay of more than 20 °C of the maximum derivated weight loss peak compared to unfilled SAN. This shows the influence of the nanoplatelets dispersion level on the thermal stability enhancement. Under helium, only the masterbatch-redispersed nanocomposite shows a thermal enhancement, but the effect is less marked than under air.

When comparing the sample thermal behaviour under air and under helium, unfilled SAN begins to degrade almost 15 °C earlier under air, because of oxidation reactions during the decomposition.²⁷ The difference is less pronounced for SAN-DM30B and disappears for SAN-MB30B. In fact, the SAN-

Table 4 Values of the maximum derivated weight peaks obtained from thermogravimetric analysis

Sample	Maximum derivated weight loss peak under air/°C	Maximum derivated weight loss peak under He/°C
SAN	418	433
SAN-DM30B	429	434
SAN-MB30B	441	439

MB30B curves under air and helium superimpose themselves quite well (not shown). Under air, the oxidation reactions usually taking place must be prevented by a barrier effect produced by the nanoclays which would have migrated at the sample surface to form a protective layer and should therefore prevent/refrain the oxidation reaction to occur.²⁸ This layer is only efficient when most of the clay sheets are exfoliated.

Clays are known for their flame retardancy capacity. During burning, the nanosheets migrate at the sample surface and form an insulating char layer that serves as a barrier to both mass and energy transfer.^{29,30} Flame retardant properties characteristic of nanoclays have been studied by mass loss cone calorimetry measurements. The data reported in Table 5 include the peak of heat release rate (PHRR), the total heat released (THR) and the time to ignition (t_{ign}). As shown graphically in Fig. 8 and with data from Table 5, the nanocomposites PHRR are decreased compared to SAN PHRR.

The effect is more pronounced for the sample with the higher extent of nanoclay delamination (SAN-MB30B), with a PHRR value decreased by almost 40%. Moreover, the THR decreases too, proving the beneficial effect of a few percent of well-dispersed nanoclay into the SAN matrix. This THR drop may be explained as follows: (i) either the barrier formed by the char might retain some of the polymer, thus decreasing the amount of SAN burned and so of the quantity of energy released, and/or (ii) the degradation pathway of SAN is modified leading to less “energetic” evolving gases.³¹ Time to ignition is not affected by the presence of clay as it remains almost constant for all the samples.

The aspect of the samples obtained after combustion also indicates the capacity of SAN-MB30B to form a stable char (Fig. 9). Unfilled SAN leaves no residue after the burning

Table 5 Values of cone calorimetry parameters realised on SAN and SAN/clay nanocomposites

Sample	Ignition time	PHRR/kW m ⁻²	THRR/mJ m ⁻²
SAN	68	495	105
SAN-DM30B	68	388	96
SAN-MB30B	74	306	83

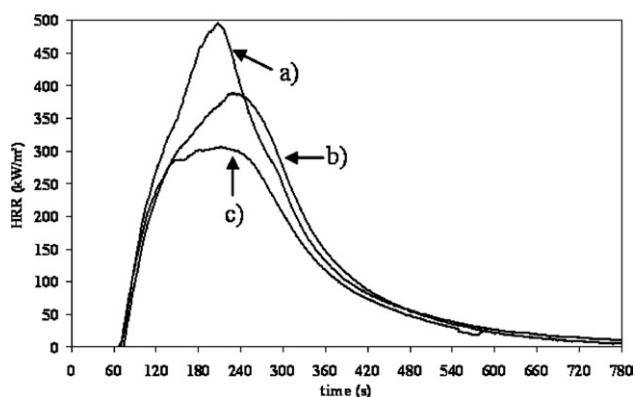


Fig. 8 Cone calorimetry curves (heat flux: 35 kW m⁻²) corresponding to a) SAN, b) SAN-DM30B and c) SAN-MB30B.

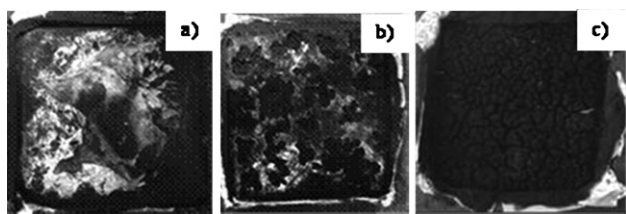


Fig. 9 Picture of the char residue recovered after cone calorimetry measurements for a) SAN, b) SAN-DM30B and c) SAN-MB30B.

experiment (Fig. 9a) whereas nanocomposite residues form a char. This char is highly cohesive and homogeneous in the case of SAN-MB30B (Fig. 9c) while SAN-DM30B residue is smaller and not cohesive at all (Fig. 9b). This shows the importance of an efficient clay exfoliation into the host matrix in order to obtain the best fire behaviour improvement.^{27,32,33}

Gas permeability

Layered silicates are known to increase gas barrier properties by creating a tortuous path for gas molecules trying to cross the sample. Gas barrier properties of nanocomposites depend on silicate particle dimensions and on the extent of dispersion of silicate layers into the polymer matrix. It has to be noted that platelets alignment maximises their effectiveness in creating a more tortuous path for gas molecules.^{34–36} We have performed gas permeability measurements on the unfilled SAN matrix and the corresponding nanocomposites, on samples pressed into thin nanocomposite films which are characterized by a different clay delamination quality. Three different gases have been chosen for these experiments, He, CO₂ and O₂. Results, reported in Fig. 10, are expressed in relative permeability, which is nanocomposite permeability divided by unfilled SAN permeability. A clear decrease in gas relative permeability is observed for the nanocomposites and the highest drop appears for the well-dispersed nanocomposite (about 50% permeability decrease), which is consistent with a higher aspect ratio (*i.e.* thinner intercalated stacks issued from the clay improved delamination) creating a more tortuous path. He and CO₂ show the same behaviour whereas gas relative permeability reduction is slightly lower with O₂.

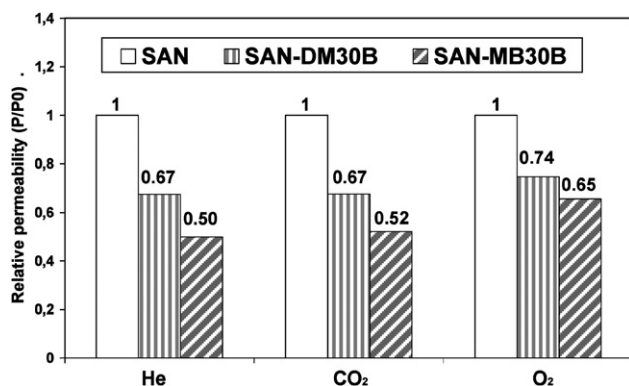


Fig. 10 Relative gas permeability of SAN and SAN/clay nanocomposites (3 wt% clay).

Conclusions

SAN/clay nanocomposites have been successfully prepared by melt-blending the polymer with highly filled PCL/clay masterbatches previously prepared by *in situ* intercalative polymerization in supercritical carbon dioxide. XRD and TEM data confirm the high degree of clay exfoliation in the masterbatch redispersed nanocomposites compared to a semi-intercalated/semi-exfoliated morphology with the presence of large intercalated aggregates in the case of direct melt-blending of the commercial clay. Tensile testing experiments performed on SAN/clay nanocomposites have shown neither reinforcement nor deterioration of the Young's modulus compared to SAN, whereas clay has a negative effect on SAN impact resistance. On the other hand, SAN permeability to gases is highly reduced with the addition of only 3 wt% of well-exfoliated nanoclays, up to 50% for helium and CO₂ and 35% for oxygen. Fire properties of nanocomposites are also greatly enhanced with a higher degradation temperature and an important decrease of heat release compared to pristine polymer matrix, thanks to the exfoliated nanoclays which form a cohesive char during combustion. This study has thus shown the superiority of masterbatch-redispersed clay over directly mixed commercial organoclay in term of clay delamination efficiency into SAN. This clay exfoliation results in an important improvement of the thermal stability and gas permeability of the nanocomposite.

Acknowledgements

CERM and CIRMAP thank the Region Wallonne in the frame of the WINNOMAT program PROCOMO. The authors are grateful to Interuniversity Attraction Poles Programme PAI P6/27 – Belgian State – Belgian Science Policy for financial support. C.D. is “Chercheur Qualifié” by F.N.R.S., Belgium.

References

- M. Alexandre and P. Dubois, *Mater. Sci. Eng.*, 2000, **28**, 1–63.
- T. D. Furness, D. L. Hunter and D. R. Paul, *Macromolecules*, 2004, **37**, 1793–1798.
- B. Lepoittevin, N. Panoustier, M. Devalckenaere, M. Alexandre, D. Kubies, C. Calberg, R. Jérôme and P. Dubois, *Macromolecules*, 2002, **35**, 8385–8390.
- M.-A. Paul, C. Delcourt, M. Alexandre, P. Degée, F. Monteverde, A. Rulmont and P. Dubois, *Macromol. Chem. Phys.*, 2005, **206**, 484–498.
- A. He, L. Wang, J. Li, J. Dong and C. C. Han, *Polymer*, 2006, **47**, 1767–1771.
- H.-W. Wang, K.-C. Chang and H.-C. Chu, *Polym. Int.*, 2005, **54**, 114–119.
- J. W. Kim, M. H. Noh, H. J. Choi, D. C. Lee and M. S. Jhon, *Polymer*, 2000, **41**, 1229–1231.
- Y. S. Choi, M. Xu and I. J. Chung, *Polymer*, 2003, **44**, 6989.
- H. A. Stretz, D. R. Paul, H. Keskkula and P. E. Cassidy, *Polymer*, 2005, **46**, 2621–2637.
- L.-L. Chu, S. K. Anderson, J. D. Harris, M. W. Beach and A. B. Morgan, *Polymer*, 2004, **45**, 4051–4061.
- B. Nam Jang, D. Wang and C. A. Wilkie, *Macromolecules*, 2005, **38**, 6533–6543.
- H. A. Stretz and D. R. Paul, *Polymer*, 2006, **47**, 8123–8136.
- M. B. Ko, *Polym. Bull.*, 2000, **45**, 183–190.
- S.-S. Lee and J. Kim, *J. Polym. Sci., Part B: Polym. Phys.*, 2005, **42**, 2367–2372.
- S. W. Kim, W. H. Jo, M. S. Lee, M. B. Ko and J. Y. Jho, *Polymer*, 2001, **42**, 9837–9842.
- A. Kiersnowski and J. Piglowski, *Eur. Polym. J.*, 2004, **40**, 1199–1207.

-
- 17 S. C. Chiu and T. G. Smith, *J. Appl. Polym. Sci.*, 1984, **29**, 1797–1814.
 - 18 B. Lepoittevin, N. Pantoustier, M. Devalckenaere, M. Alexandre, C. Calberg, R. Jérôme, C. Henrist, A. Rulmont and P. Dubois, *Polymer*, 2003, **44**, 2033–2040.
 - 19 L. Urbanczyk, C. Calberg, F. Stassin, M. Alexandre, R. Jérôme, C. Jérôme and C. Detrembleur, *Polymer*, 2008, **49**, 3979–3986.
 - 20 S. Benali, S. Peeterbroeck, P. Brocorens, F. Monteverde, L. Bonnaud, M. Alexandre, R. Lazzaroni and Ph. Dubois, *Eur. Polym. J.*, 2008, **44**, 1673–1685.
 - 21 H. A. Stretz, D. R. Paul and P. E. Cassidy, *Polymer*, 2005, **46**, 3818–3830.
 - 22 B. Lepoittevin, M. Devalckenaere, N. Pantoustier, M. Alexandre, D. Kubies, C. Calberg, R. Jérôme and P. Dubois, *Polymer*, 2002, **43**, 4017–4023.
 - 23 M. Tanniru, Q. Yuan and R. D. K. Misra, *Polymer*, 2006, **47**, 2133–2146.
 - 24 W. J. Jackson and J. R. Caldwell, *J. Appl. Polym. Sci.*, 1967, **11**, 211–226.
 - 25 M. Shuster and M. Narkis, *Polym. Eng. Sci.*, 1994, **34**, 1613–1618.
 - 26 S. L. Anderson, E. A. Grulke, P. T. DeLassus, P. B. Smith, C. W. Kocher and B. G. Landes, *Macromolecules*, 1995, **28**, 2944–2954.
 - 27 B. N. Jang and C. A. Wilkie, *Polymer*, 2006, **46**, 9702–9713.
 - 28 M. C. Costache, M. J. Heidecker, E. Manias, G. Camino, A. Frache, G. Beyer, R. K. Gupta and C. A. Wilkie, *Polymer*, 2007, **48**, 6532–6545.
 - 29 S. Bourbigot, J. W. Gilman and C. A. Wilkie, *Polym. Degrad. Stab.*, 2004, **84**, 483–492.
 - 30 H. A. Stretz, W. Wootan, P. E. Cassidy and J. H. Koo, *Polym. Adv. Technol.*, 2005, **16**, 239–248.
 - 31 B. N. Jang, M. Costache and C. A. Wilkie, *Polymer*, 2005, **46**, 10678–10687.
 - 32 S. Bourbigot, D. L. Vanderhart, J. W. Gilman, S. Bellayer, H. A. Stretz and D. R. Paul, *Polymer*, 2004, **45**, 7627–7638.
 - 33 J. Zhang, D. D. Jiang, D. Wang and C. A. Wilkie, *Polym. Degrad. Stab.*, 2006, **91**, 2665–2674.
 - 34 L. E. Nielsen, *J. Macromol. Sci., Pure Appl. Chem.*, 1967, **A1**(5), 929–942.
 - 35 R. K. Bharadwaj, *Macromolecules*, 2001, **34**, 9189–9192.
 - 36 M. A. Osman, V. Mittal and H. R. Lusti, *Macromol. Rapid Commun.*, 2004, **25**, 1145–1149.